

Article

Adsorption and Separation of Crystal Violet, Cerium(III) and Lead(II) by Means of a Multi-Step Strategy Based on K10-Montmorillonite

Filippo Parisi ^{1,2} 

¹ Dipartimento di Fisica e Chimica, Università degli Studi di Palermo Viale delle Scienze, pad. 17, 90128 Palermo, Italy; filippo.parisi@unipa.it

² Consorzio Interuniversitario Nazionale per la Scienza e Tecnologia dei Materiali, INSTM, Via G. Giusti, 9, 50121 Florence, Italy

Received: 14 April 2020; Accepted: 19 May 2020; Published: 20 May 2020



Abstract: A multi-step procedure, based on the employment of K10-Montmorillonite, is proposed for the selective removal of metal ions and dyes from a multicomponent solution. The objective is twofold: decontaminate the effluents and separate and recover the valuable byproducts present in wastewaters. Three common contaminants, i.e., crystal violet dye (CV), Ce(III) and Pb(II) were chosen as “model” pollutants. The main factors affecting the pollutants’ sorption were investigated. The experimental data were correlated with adsorption isotherms and kinetic models to obtain a deeper insight into the adsorption processes. The affinity of the clay toward the pollutants is favored by an increasing pH and follows the order CV > Pb(II) > Ce(III). Whereas Ce(III) metal ions do not adsorb onto clay under strongly acidic conditions, both Pb(II) and CV can adsorb under all the investigated pH conditions. The analysis of isotherms and kinetic profiles revealed that CV adsorbs onto clay through a mechanism consisting of two parallel processes, namely cation exchange on the external mineral surface and in the interlayer and surface complexation at the edge sites, while metal ion uptake is due solely to cation exchange processes involving mineral surfaces. The time required for the complete removal of pollutants follows the order CV > Ce(III) >> Pb(II). The possibility to modulate the adsorption features by changing experimental conditions was successfully employed to propose the best strategy for the progressive removal of different components from aqueous solutions.

Keywords: clay; adsorption; montmorillonite; wastewaters; pollutants; dyes; metal ions

1. Introduction

Water effluents are very complex systems that usually contain different kinds of pollutants. The modern approach to water remediation requires the development of “green” and economically sustainable strategies which allow for the selective removal of the contaminants and provide the possibility of recovering and reusing them [1–5].

Adsorption technology was revealed as a very effective strategy for the disposal of several kinds of pollutants [6–15].

In this regard, researchers are increasingly interested in clay minerals which are biocompatible, non-toxic, cost effective and efficient [16–20]. In the present paper, the employment of a K10-montmorillonite clay mineral (K10-Mt) is proposed as versatile sorbent for three classes of pollutant, namely dyes, rare earth and heavy metals. Among the most hazardous contaminants, dyes and metals are widely released from industrial activities and represent two of the most widespread causes of water pollution, due to their toxic potential and their recalcitrant capacity [21–33].

The choice of montmorillonite as sorbent was related to the extensive literature dealing with the investigation and exploitation of this mineral clay for environmental applications [34–38]. The present

paper represents the continuation of a previous work by Parisi et al. [39], where the performances of montmorillonite clay in the removal and separation of contaminants from a binary mixture, containing the crystal violet dye (CV) and the Ce(III) metal ion, were investigated. In light of the promising results, the study was here extended to a ternary mixture containing, in addition to the aforementioned CV and Ce(III), the Pb(II) metal ion as model for heavy metals.

All the investigated contaminants are in the cationic form in a wide range of pH values. The estimated pKa values of crystal violet are indeed 5.31 and 8.64 [40], indicating that this compound will exist almost entirely in the cation form in the environment.

Beside their role as representative exponents of the three classes of compounds, the contaminants were selected since they are all largely employed in several applications and widely released from industrial activities [41–47]. Therefore, the probability of finding the three classes of contaminants in sewage effluents and rivers close to industrial areas is certainly high. In addition, their toxic effect on human health is well documented, which makes their disposal an important environmental issue [48–52]. Moreover, the high versatility of the K10-Mt clay provides the possibility of progressively removing the pollutants in order to separate and reuse them, thus accomplishing the twofold objective to decontaminate and fully exploit the effluents.

Although adsorption strategies were widely applied in the removal of metal cations and dyes [53–58], a systematic study with the aim of developing an efficient procedure for the selective removal and separation/recovery of the three classes of compounds in a multicomponent mixture is still lacking.

In the first part of the present work, the adsorption of the three components separately was investigated. Batch experiments were performed to evaluate the influence of various experimental parameters like pH conditions, initial amounts of pollutants and clay. Adsorption isotherms and kinetic profiles were then investigated in order to obtain a deeper insight into the adsorption processes and to establish the most effective strategy to modulate the adsorption of the different pollutants.

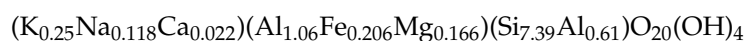
Then, based on the obtained information, a multi-step procedure was tested to selectively remove the three components from a ternary mixture mimicking a real effluent.

2. Materials and Methods

2.1. Materials

K10-montmorillonite (K10-Mt), crystal violet (CV, $C_{25}H_{30}ClN_3$, $M_w = 407.99 \text{ g}\cdot\text{mol}^{-1}$), cerium nitrate hexahydrate (Ce(III)), lead nitrate (Pb(II)), hydrochloric acid (HCl) and sodium hydroxide (NaOH) standard solutions were from Sigma Aldrich and they were used as received. K10-Mt is an acid treated montmorillonite with a partially destroyed structure [59]. The BET surface area is $220 \text{ m}^2\cdot\text{g}^{-1}$, the CEC is $119 \text{ meq}/100 \text{ g}$, the total pore volume is $0.3 \text{ cm}^3\cdot\text{g}^{-1}$ and the average pore size is 6.25 nm .

The structural formula is as follows:



2.2. Preparation of Pollutant/Clay Composites: Equilibrium and Kinetic Experiments

Pollutant stock solutions and K10-Mt suspensions were prepared by weighing the proper amounts of the components and dissolving them in HCl or NaOH solutions at the required pH (2.0, 4.0, 6.0, 8.0). The clay dispersions were stirred for about 2 h before use.

Hybrid materials at different pH values were prepared by adding appropriate aliquots of the aqueous solution of pollutants to the aqueous K10-Mt dispersion. The obtained dispersion was stirred for 2 h, then centrifuged 1 h at 10,000 rpm using a Centra MP4R IEC centrifuge (International Equipment Company, Needham Heights, MA, USA). The obtained supernatants were separated from the solid and spectrophotometrically analyzed by registering the UV-Vis spectra with a diode array Analytic Jena S600 spectrophotometer (Analytik Jena, Jena, Germany) equipped with thermostated

compartments for cuvettes with optical path lengths (l) of both 1 and 5 cm, and a magnetic stirring apparatus. The UV-Vis absorbance values (A) were used to determine the residual concentration of the contaminants (C) after the treatment with the clay, using the Lambert–Beer law ($A = \epsilon \times l \times C$). The molar adsorption coefficient values (ϵ) of CV, Pb(II) and Ce(III) at two different pH conditions were determined by constructing the calibration curves (Table 1).

Table 1. Molar adsorption coefficient values ($\epsilon/\text{M}^{-1}\cdot\text{cm}^{-1}$) of crystal violet dye (CV), Pb(II) and Ce(III) at pH 2.0 and 6.0.

Molar Adsorption Coefficient	pH 2.0		pH 6.0	
	$\epsilon/\text{M}^{-1}\cdot\text{cm}^{-1}$	R^2	$\epsilon/\text{M}^{-1}\cdot\text{cm}^{-1}$	R^2
CV ($\lambda_{\text{max}} = 591 \text{ nm}$)	$89,000 \pm 3000$	0.99627	$75,000 \pm 2000$	0.99587
Pb(II) ($\lambda_{\text{max}} = 207 \text{ nm}$)	$37,000 \pm 4000$	0.99464	$27,200 \pm 800$	0.99954
Ce(III) ($\lambda_{\text{max}} = 253 \text{ nm}$)	750 ± 30	0.99852	850 ± 40	0.99753

Aiming at evaluating the minimum amount of clay required for the complete removal of the pollutants under the different conditions, experiments were performed by keeping the concentration of contaminants constant ($20 \text{ mg}\cdot\text{dm}^{-3}$ and $60 \text{ mg}\cdot\text{dm}^{-3}$) and changing the amount of mineral clay in the range $0.05\text{--}1.6 \text{ g}\cdot\text{dm}^{-3}$. The effect of pH was investigated by carrying out experiments in the pH range from 2.0 to 8.0. When necessary, the supernatants of Pb(II) and CV were opportunely diluted, while, for Ce(III) solutions, due to the very low ϵ value, long path cuvettes (optical path lengths 5 cm) were employed.

In order to construct the adsorption isotherms, the concentration of the pollutants was changed in the range $2\text{--}300 \text{ mg}\cdot\text{dm}^{-3}$ at a constant amount of K10-Mt ($0.4 \text{ g}\cdot\text{dm}^{-3}$).

Kinetic adsorption profiles were studied under constant stirred conditions at $25.0 \text{ }^\circ\text{C}$ by monitoring the UV-Vis spectrum evolution of aqueous solutions of pollutants in the presence of K10-Mt by using an Analytic Jena S600 diode array spectrophotometer. The initial concentration of the contaminants was chosen in order to obtain reasonable absorbance values ($10 \text{ mg}\cdot\text{dm}^{-3}$ for CV and Pb(II) and $50 \text{ mg}\cdot\text{dm}^{-3}$ for Ce(III)). In all cases, the amount of clay was chosen in order to ensure the total removal of them. Since it is known from the literature [52] that the coalescence of the montmorillonite particles could slightly influence the absorbance reduction, this process was also monitored spectrophotometrically and automatically subtracted point by point from the kinetic adsorption profiles.

3. Results and Discussion

3.1. Effect of Experimental Parameters: pH Value, Initial Concentration of Adsorbate, Amount of Sorbent

Batch experiments were performed to evaluate the influence of various experimental parameters onto sorption processes.

Figures 1 and 2 report the adsorption capacity values of the pollutants as a function of the amount of clay in terms of both the amount of adsorbed pollutant per gram of clay (Q_e) and the percentage of sorption. Two different values of pH (namely pH 2.0 and pH 6.0) and two different values of sorbate initial concentration were analyzed.

These preliminary experiments allow for the determination of the amount of clay required for the complete removal of the different pollutants (100% sorption) under different experimental conditions.

As clearly evidenced in the figures, the equilibrium sorption capacity, Q_e , which actually represents the pollutant/clay ratio, ensuring the complete adsorption of the species, follows the order $\text{CV} > \text{Pb(II)} > \text{Ce(III)}$. As for the Ce(III), as already observed in [39], under strongly acidic conditions no adsorption

onto K10-Mt is detected. Moreover, an increase in the sorption capacity with the increasing pH is detected, as is better evidenced in Figure 3.

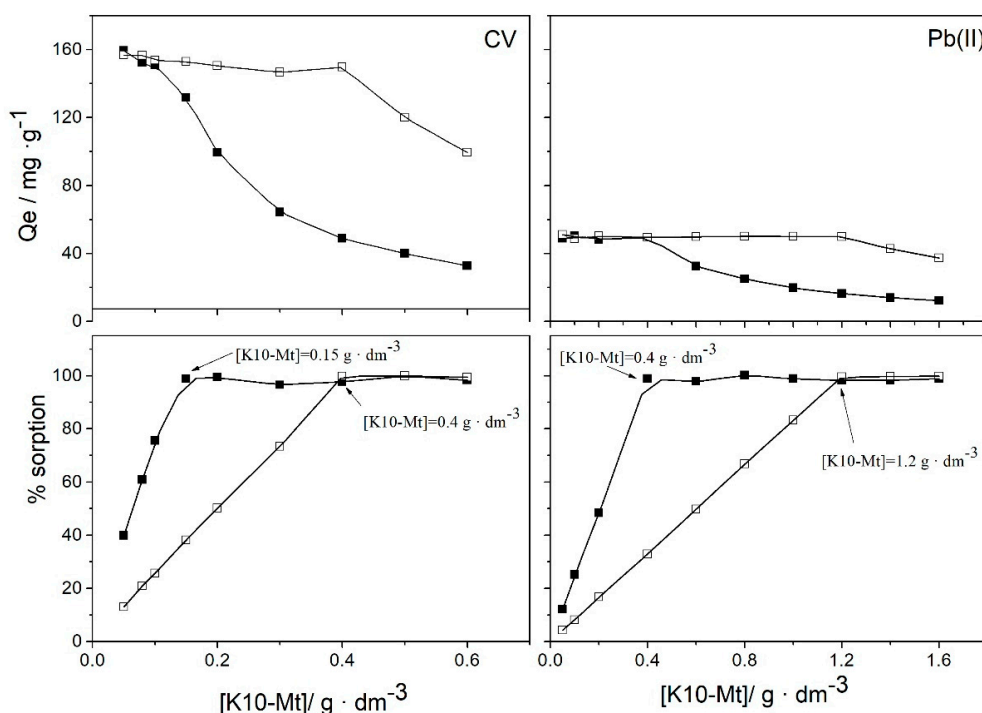


Figure 1. Sorption capacity of pollutants as a function of the amount of clay at pH 2.0. $C_0 = 20 \text{ mg} \cdot \text{dm}^{-3}$ (■) and $C_0 = 60 \text{ mg} \cdot \text{dm}^{-3}$ (□). The amount of clay required for the complete adsorption of contaminants is indicated by the arrows in the graph.

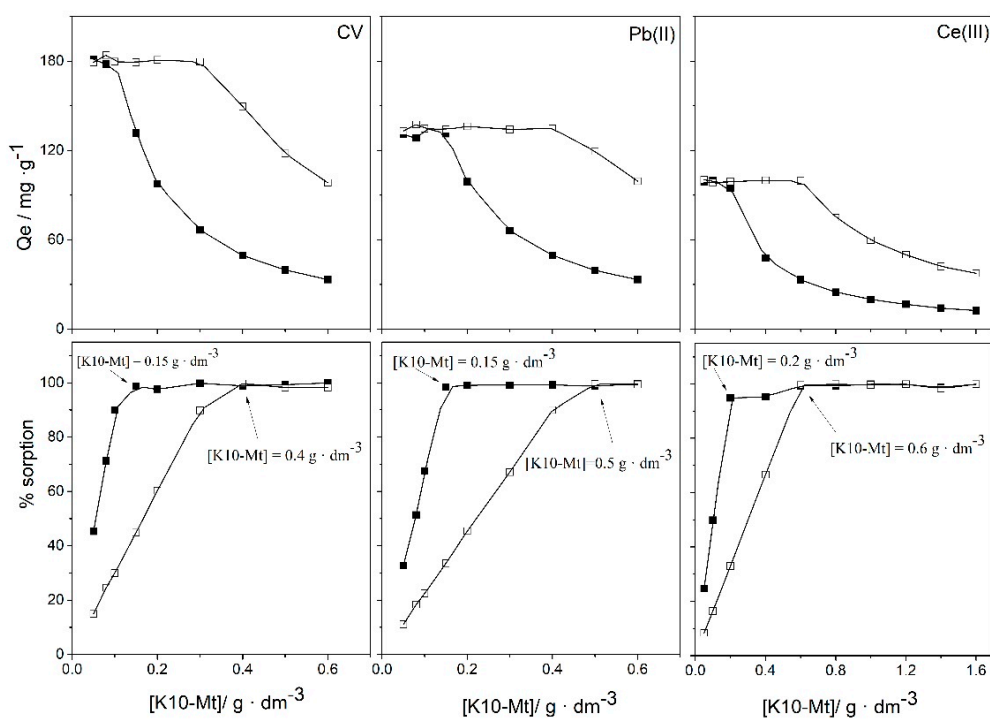


Figure 2. Sorption capacity of pollutants as a function of the amount of clay at pH 6.0. $C_0 = 20 \text{ mg} \cdot \text{dm}^{-3}$ (■) and $C_0 = 60 \text{ mg} \cdot \text{dm}^{-3}$ (□). The amount of clay required for the complete adsorption of contaminants is indicated by the arrows in the graph.

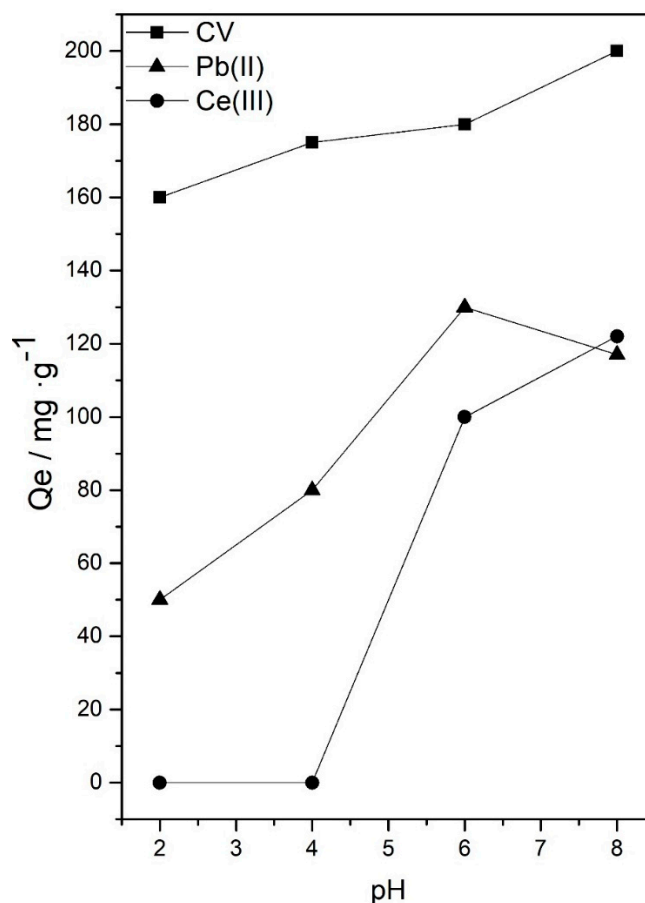


Figure 3. Adsorption capacity of pollutants as a function of pH.

The increase in the adsorption capacity of cationic species with the increasing pH is in line with the literature [36,39] and is attributable to the deprotonation of hydroxyls, which produces a larger negative charge to compensate. The lack of adsorption of Ce(III) at an acidic pH seems to indicate the strong influence of electrostatic repulsions between H^+ ions and the metal cations.

3.2. Adsorption Isotherms

A deeper understanding of the adsorption processes can be achieved through an investigation of the adsorption isotherms, as reported in Figure 4.

The sorption parameters obtained from the application of the classical Langmuir and Freundlich models are collected in Table 2.

The Akaike information criteria (AIC), the coefficient of multiple determination (R^2) and the analysis of the residuals (Supplementary Materials, Figure S1) were used as statistical criteria to determine the most reliable model [53].

The most reliable model was chosen on the basis of the lower AIC value, the R^2 value closest to unity and the higher randomness of the results in the residual plot.

According to Parisi et al. [39], the Freundlich model, which implies the heterogeneity of the adsorption sites, proved to be the most reliable for the uptake of CV. The Langmuir model better reproduces the adsorption isotherm of both Pb(II) and Ce(III), indicating the presence of a single adsorption site for the metal ion uptake. It can be argued therefore that both cation exchange processes and electrostatic interaction with the clay surface occur in the case of CV adsorption, while the second process is solely responsible for the metal ion uptake.

Although the adsorption parameters obtained for dye and metals do not allow for a direct comparison, Figure 4 and data reported in Table 2 confirm the already-reported trend for the adsorption capacity (CV > Pb(II) > Ce(III)).

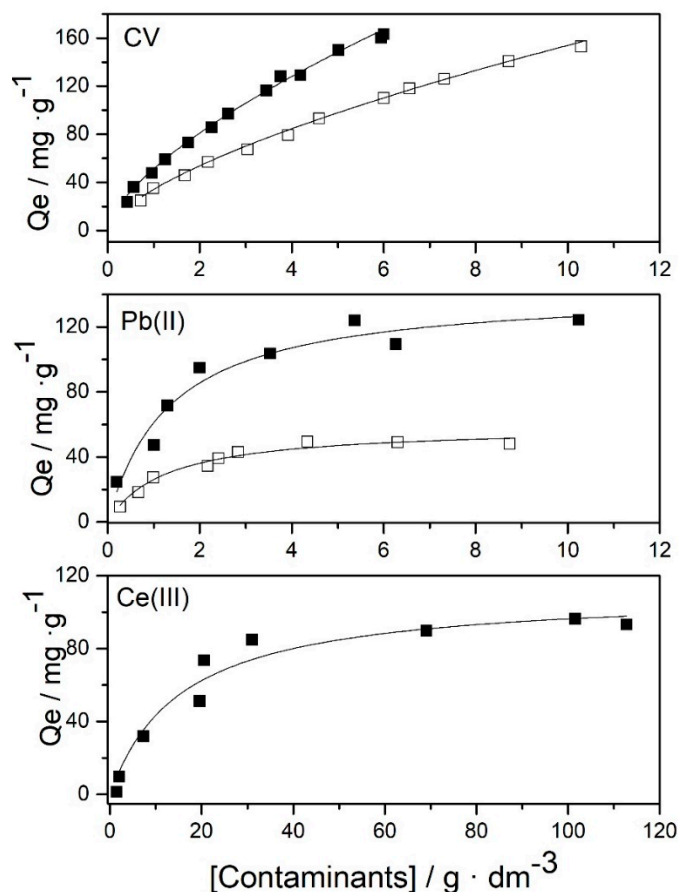


Figure 4. Adsorption isotherm of CV, Pb(II) and Ce(III) onto K10-montmorillonite clay mineral (K10-Mt) performed at pH = 6.0 (■) and pH = 2.0 (□). Lines correspond to the fit by Freundlich model for CV and Langmuir model for metals ions, respectively.

Table 2. Sorption parameters for the adsorption isotherms of the contaminants onto K10-Mt.

Contaminants	Langmuir $Q_e = \frac{q_m \cdot K_L \cdot C}{1 + K_L \cdot C}$			Freundlich $Q_e = K_F \cdot C^{1/n}$		
	Sorption Parameters	pH 2.0	pH 6.0	Sorption Parameters	pH 2.0	pH 6.0
CV	K_L $dm^3 \cdot mg^{-1}$	0.105 ± 0.01	0.18 ± 0.02	K_F $(mg \cdot g^{-1})$ $(dm^3 \cdot mg^{-1})^{1/n}$	33.3 ± 0.8	50 ± 1
	q_m $mg \cdot g^{-1}$	290 ± 20	300 ± 18	n	1.51 ± 0.03	1.51 ± 0.01
Pb(II)	K_L $dm^3 \cdot mg^{-1}$	0.8 ± 0.1	0.8 ± 0.1	K_F $(mg \cdot g^{-1})$ $(dm^3 \cdot mg^{-1})^{1/n}$	26 ± 2	67 ± 6
	q_m $mg \cdot g^{-1}$	59 ± 3	141 ± 6	n	2.88 ± 0.05	3.8 ± 0.6
Ce(III)	K_L $dm^3 \cdot mg^{-1}$		0.06 ± 0.02	K_F $(mg \cdot g^{-1})$ $(dm^3 \cdot mg^{-1})^{1/n}$		23 ± 6
	q_m $mg \cdot g^{-1}$		110 ± 8	n		3.4 ± 0.6

Additional information about the adsorption mechanism was obtained through the application of the Dubinin–Radushkevich (DR) equation (Figure 5):

$$\ln Q_e = \ln X_m - k\varepsilon^2$$

where $\varepsilon = RT \ln(1 + 1/C_e)$, R ($\text{KJ}\cdot\text{mol}^{-1} \text{K}^{-1}$) the gas constant, T (K) the absolute temperature, X_m ($\text{mol}\cdot\text{g}^{-1}$) the clay adsorption capacity and k ($\text{mol}^2\cdot\text{KJ}^{-2}$) the DR isotherm constant related to the adsorption energy through the equation:

$$E = 1/(2k)^{1/2}$$

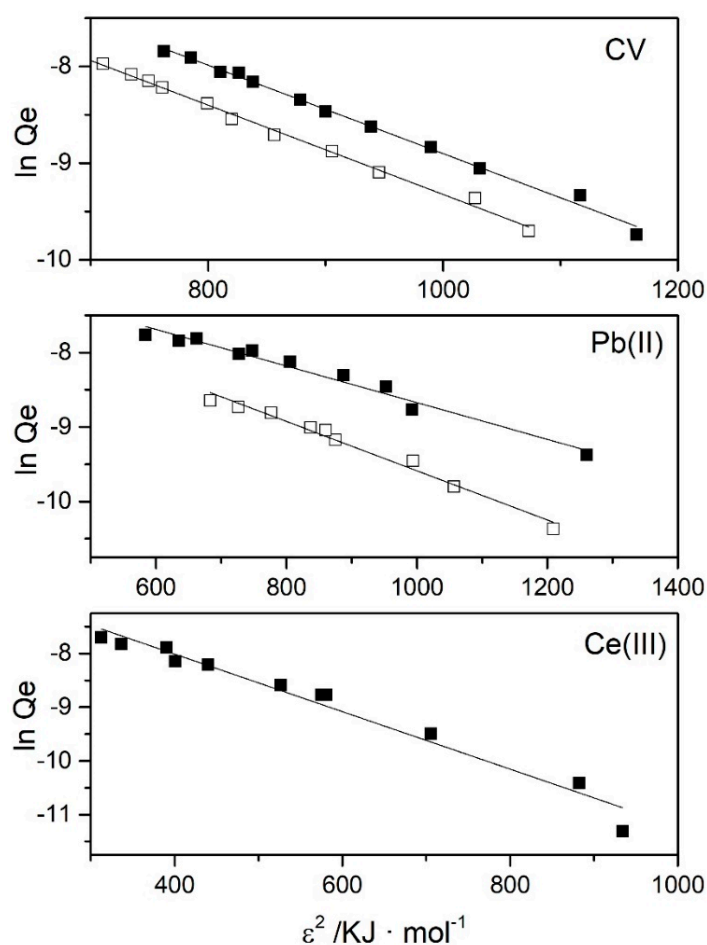


Figure 5. Dubinin–Radushkevich (DR) adsorption isotherms of CV, Pb(II) and Ce(III) onto K10-Mt performed at pH = 6.0 (■) and pH = 2.0 (□). Lines correspond to the fit by DR model.

The sorption DR parameters are reported in Table 3.

Perusal of the data reported in Table 3 indicates that the obtained energy values are in the range 8–16 $\text{kJ}\cdot\text{mol}^{-1}$, which, according to the literature [60], is characteristic of adsorption processes dominated by the cation exchange mechanism. The capability of metal ions and cationic dyes to compete with the montmorillonite counterions is well documented in the literature [61,62].

Table 3. Sorption DR parameters for the adsorption isotherms of the contaminants onto K10-Mt.

		$X_m/\text{mol}\cdot\text{g}^{-1}$	$k/\text{mol}^2\cdot\text{kJ}^{-2}$	$E/\text{kJ}\cdot\text{mol}^{-1}$	R^2
Pb	pH = 2.0	$(1.88 \pm 0.04)\cdot 10^{-3}$	$(3.29 \pm 0.2)\cdot 10^{-3}$	12.3 ± 0.7	0.971
	pH = 6.0	$(2.00 \pm 0.04)\cdot 10^{-3}$	$(2.5 \pm 0.2)\cdot 10^{-3}$	14 ± 1	0.968
CV	pH = 2.0	$(1.08 \pm 0.02)\cdot 10^{-2}$	$(4.6 \pm 0.1)\cdot 10^{-3}$	10.4 ± 0.1	0.996
	pH = 6.0	$(1.31 \pm 0.03)\cdot 10^{-2}$	$(4.6 \pm 0.1)\cdot 10^{-3}$	10.4 ± 0.2	0.994
Ce(III)	pH = 6.0	$(2.82 \pm 0.09)\cdot 10^{-3}$	$(5.5 \pm 0.4)\cdot 10^{-3}$	9.5 ± 0.7	0.953

3.3. Kinetic Measurements

Kinetic adsorption profiles are reported in Figure 6 for all the investigated contaminants at two different pH values. First of all, it can be observed that the chosen values of pollutant/clay ratios ensure the achievement of the complete adsorption of the species (100% sorption).

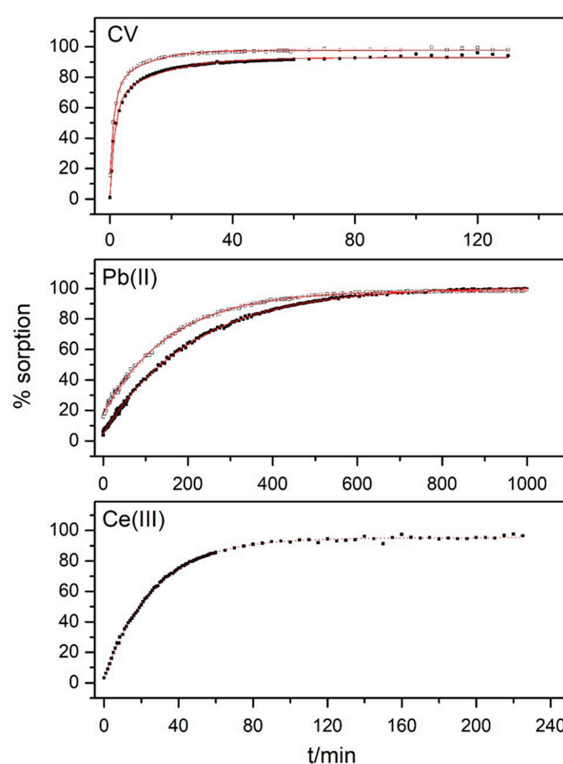


Figure 6. Kinetic profiles for the adsorption of CV, Pb(II) and Ce(III) onto K10-Mt at pH 6.0 (■) and pH = 2.0 (□).

First-order and double exponential kinetic models (DEM) were applied to fit the experimental data (the reader can refer to [52] and references therein for a detailed explanation of the models).

The rate equation for the first order and DEM model are described by the following equations:

First order model $Q_t = Q_e - A \exp(-kt)$;

DEM model $Q_t = Q_e - A_1 \exp(-k_1 t) - A_2 \exp(-k_2 t)$.

Analogously to the procedure applied for the analysis of the equilibrium data, the discrimination among the different models was performed using the statistical criteria and the analysis of the residuals reported in the Supplementary Materials, Figure S2.

The DEM model, which describes a mechanism consisting of two parallel reactions [6,35,54–56], revealed the most reliable results for the CV adsorption process, while Pb(II) and Ce(III) adsorb onto K10-Mt clay through a simple first order model. These results can be taken as further proof of the results of the adsorption isotherms, showing the presence of different adsorption sites available for

CV uptake and a single adsorption site for metal ion uptake. Table 4 reports the kinetic rate constant values obtained by applying the correct models to the experimental data.

Table 4. Rate constant values for pseudo-first order and double exponential models applied to the kinetic profiles of adsorption of the pollutants onto K10-Mt.

		pH 2.0	pH 6.0
CV	k_1/min^{-1}	0.74 ± 0.03	0.62 ± 0.03
	k_2/min^{-1}	0.095 ± 0.005	0.063 ± 0.004
Pb(II)	k/min^{-1}	0.00632 ± 0.00003	0.00469 ± 0.00002
Ce(III)	k/min^{-1}		0.0376 ± 0.0003

Data reported in Table 4 indicate that the values of the kinetic rate constants slightly diminish with a pH increase, which is easily attributable to the higher amount of adsorbed pollutants, which means that more time is required to reach the saturation conditions.

Moreover, it is worth noting that, although lead(II) and crystal violet are both able to adsorb onto K10-Mt at an acidic pH, the processes occur at very different timescales, which seems to indicate the higher affinity of the dye toward the clay in comparison with the metal ion. With the aim of finding the optimal conditions for the separation of the investigated contaminants, the kinetic profile of the adsorption onto K10-Mt at pH 2.0 of the two species simultaneously present in the solution was investigated. Figure 7 reports the spectra of a solution containing Pb(II) and CV ($\sim 10 \text{ mg}\cdot\text{dm}^{-3}$) treated with $0.2 \text{ g}\cdot\text{dm}^{-3}$ K10-Mt for different time values corresponding to the adsorption process.

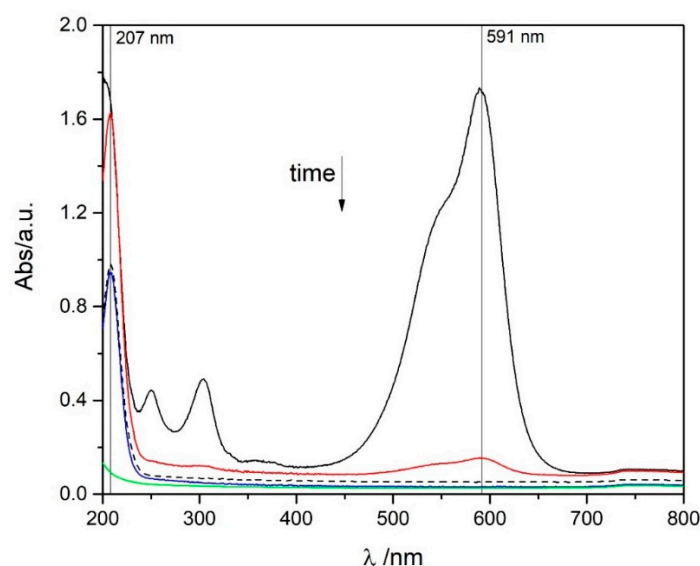


Figure 7. UV-Vis spectra of a mixture of Pb(II) and CV (10 mg dm^{-3}) before (black line) and after the treatment with K10-Mt at pH 2.0 for 20 min (red line), 60 min (blue line) and 12 h (green line). Dotted line is the UV-Vis spectrum of a solution $10 \text{ mg}\cdot\text{dm}^{-3}$ of Pb(II).

During the first 60 min of the adsorption process, a decrease in both peaks at 591 nm and 207 nm (corresponding to CV and Pb(II), respectively) can be detected. Since the adsorption peak of Pb(II) at 207 nm is actually hidden by the broad UV-adsorption of CV, the interpretation of the experiments is not trivial. For the sake of clarity, the UV-Vis spectrum of a solution $10 \text{ mg}\cdot\text{dm}^{-3}$ (dotted curve) is also reported in the figure. A comparison with the spectrum of Pb(II) indicates that only CV adsorbs onto clay during the first 60 min of the reaction and the adsorption of the metal ion starts when CV is completely removed from the solution. The whole elimination of lead from the solution is then accomplished after 12 h.

The wavelengths at λ_{\max} for Pb(II) and CV were selected and used to construct the kinetic profiles of the pollutant's adsorption onto clay from a mixture (Figure 8). In order to eliminate the contribution of CV adsorption at 207 nm, the following procedure was applied: two experiments were performed simultaneously, i.e., adsorption of CV and lead from a mixture (A) and adsorption of CV from a solution containing just the dye (B). The kinetic profile corresponding to process B was subtracted from A, point by point, in order to delete the contribution of CV in the UV region where lead (II) adsorbs.

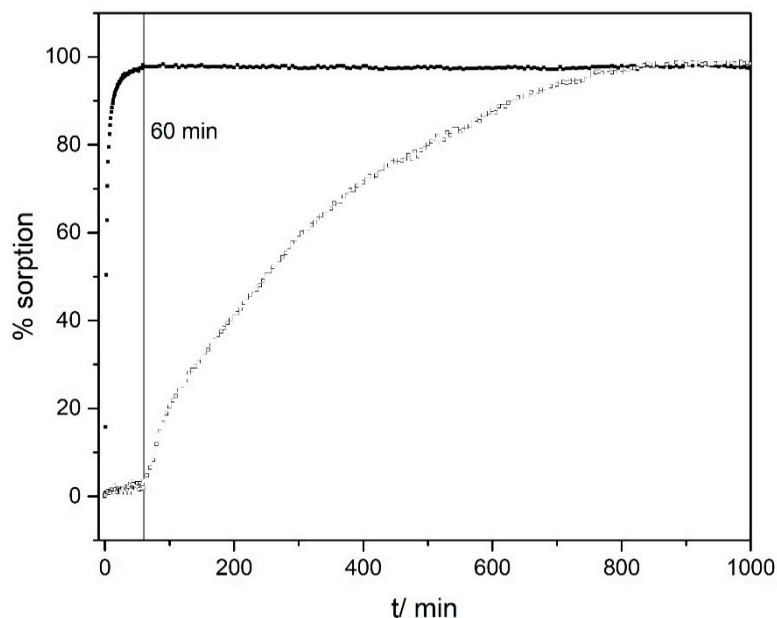


Figure 8. Kinetic profiles of Pb(II) (□) and CV (■) adsorption onto K10-Mt clay from a mixture.

The kinetic profile of lead(II) adsorption shows the presence of an “induction period” of about 60 min, corresponding to the time required for the complete removal of CV, thus indicating the higher affinity of the dye toward the clay. In other words, when simultaneously present in a mixture, the competition between the two contaminants hamper the adsorption of Pb(II).

3.4. XRD Characterization

The structural characterization of pristine and modified K10-Mt complexes was performed by means of XRD measurements (Figure 9).

The XRD patterns of the clay samples showed the presence of a very weak and broad reflection $d(001)$ at $2\theta \sim 5^\circ$ ($d = 17.6 \text{ \AA}$), characteristic of montmorillonite clay minerals, and a sharp peak at $2\theta \sim 8.9^\circ$ ($d = 9.9 \text{ \AA}$), indicating the presence of a clay mineral of the mica group (muscovite). The presence of quartz was also recognized. According to the literature [63] the weak intensity and broad peak profile of the Mt $d(001)$ reflection is due to internal disorder, and is not necessarily indicative of low phase proportion.

A comparison between the diffraction patterns of the complexes and pristine K10-Mt indicates that the clay structure is maintained during the adsorption processes.

No changes are detected in the peak positions due to the presence of metal ions, thus indicating that Ce(III) and Pb(II) ions do not enter the clay interlayer. This is consistent with the behavior already observed by different authors [64–67], which suggests that the uptake of metal cations onto montmorillonite mainly involves the outer surface of the clay.

As for the CV pollutant, small shifts in the peak position can be observed in the diffraction pattern, thus indicating the entrance of the dye onto the clay interlayer. In order to provide a better view of these effects, in Figure 10, the superimposition of the smoothed XRD patterns in the very low angle region is reported.

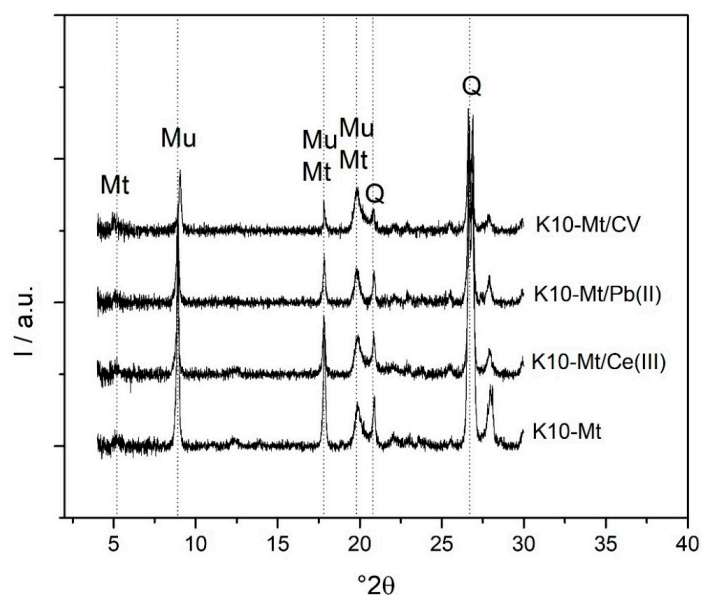


Figure 9. XRD patterns of pristine K10-Mt and K10-Mt/pollutants complexes. Montmorillonite (Mt), muscovite (Mu), quartz (Q).

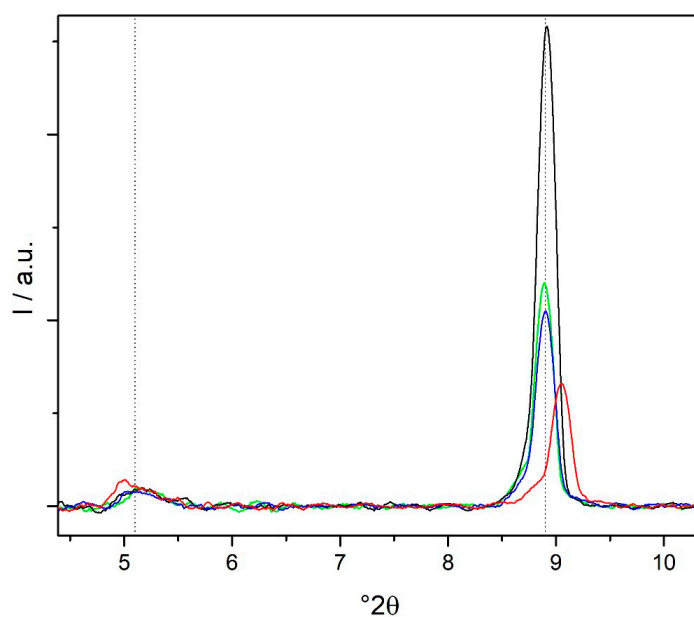


Figure 10. Superimposition of the smoothed XRD patterns in the low angle region for K10-Mt (black line) K10-Mt/CV (red line), K10-Mt/Pb (II) (green line) and K10-Mt/Ce(III) (blue line).

According to Parisi et al. [39], a slight contraction in the mica basal interlayer ($d \sim 9.9 \text{ \AA}$) and a small contraction in the Mt interlayer ($d \sim 17.6 \text{ \AA}$) are observed. The lower interplanar distance after dye adsorption could be taken as an indication of the occurrence of cation exchange processes which displace cations from the interlayer spaces.

3.5. Removal and Separation of Pollutants

The information about the equilibrium and kinetic behavior of the pollutants under the different experimental conditions was exploited to develop a procedure for the removal and separation of the different species from a solution containing the contaminants.

The proposed protocol can be resumed as follows:

- First treatment of the mixture with K10-Mt at a strongly acidic pH over a short timescale (~60 min);
- Centrifugation and separation of the CV/clay composite;
- Second treatment of the supernatant with K10-Mt at a strongly acidic pH over a long timescale (>12 h);
- Centrifugation and separation of the Pb(II)/clay composite;
- Treatment of the remaining solution (containing Cerium ions) with K10-Mt at higher pH values (>6.0);
- Centrifugation and separation of the Ce(III)/clay composite.

The amount of pollutants was chosen by taking into account the extinction coefficient values of the different species (10 mg·dm⁻³ for CV and Pb(II) and 150 mg·dm⁻³ for Ce(III)) and K10-Mt was added in excess to obtain the complete removal.

Figure 11 reports the spectra of the solution containing the three contaminants before (A) and after each treatment. For the sake of clarity, the spectra of the solutions of every single component are also reported.

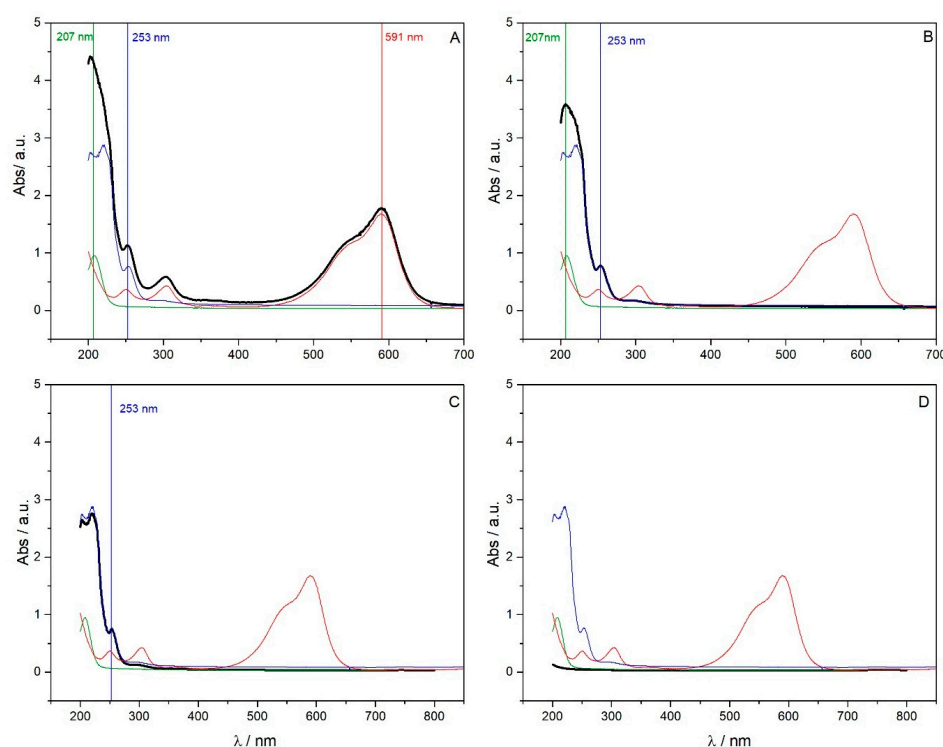


Figure 11. UV-vis spectra of a mixture (black curves) containing CV, Pb(II) and Ce(III) before (A) and after the treatment with K10-Mt (0.2 g·dm⁻³) at pH 2.0 for 60 min (B), the subsequent treatment with K10-Mt (0.2 g·dm⁻³) at pH 2.0 for 12 h (C) and after the final treatment with K10-Mt (2 g·dm⁻³) at pH 6.0 (D). Red, green and blue curves are the spectra of CV, Pb(II) and Ce(III), respectively.

The spectrum of the supernatant reported in Figure 11B is indicative of the complete removal of the CV dye, after the treatment with K10-Mt at an acidic pH for 60 min. The successful removal of lead (II) after the subsequent treatment at an acidic pH for a longer time period (12 h) is proven by the spectrum reported in Figure 11C. Finally, the addition of K10-Mt at a higher pH value leads to the elimination of the Ce(III) metal ions.

The proposed multi-step strategy was therefore efficient for the separation and removal of pollutants of a different nature from a multicomponent solution.

4. Conclusions

In this study, the adsorption features of montmorillonite mineral clay were employed for the selective removal of “model” contaminants from a ternary aqueous mixture. Three widespread toxic pollutants, i.e., crystal violet, Ce(III) and Pb(II) metal ions, were chosen as representative exponents of dyes, rare earth and heavy metals.

The effects of different variables, i.e., pollutant concentration, amount of clay, pH and contact time were investigated. The adsorption processes of the single pollutants from simplified systems were analyzed by constructing the adsorption isotherms and the kinetic profiles. Significant differences in the adsorption behavior of the three species under the different experimental conditions were recognized. First of all, both Pb(II) and CV are able to adsorb onto clay under all the investigated pH conditions, while Ce(III) metal ions do not adsorb under strongly acidic conditions. The affinity of the clay to the pollutants is always favored by increasing pH values and follows the order CV > Pb(II) > Ce(III). The adsorption mechanism of the CV dye consists of different parallel processes, i.e., cation exchange processes and surface complexation involving both the clay interlayer and the montmorillonite surface and edges, while metal cations are held to the montmorillonite through cation exchange processes involving just the clay surface. Finally, the time required for the complete removal of pollutants follows the order CV > Ce(III) >> Pb(II).

The obtained results evidence the possibility of modulating the adsorption features by changing the experimental conditions and were employed to propose a successful approach for the progressive removal of the three different species from a multicomponent mixture. This can be viewed as a launching pad for the development of a strategy for the simultaneous decontamination and valorization of real samples of water effluents.

Supplementary Materials: The following are available online at <http://www.mdpi.com/2075-163X/10/5/466/s1>, Figure S1: Residuals plot for the adsorption isotherms reported in Figure 4, fitted by using the Langmuir and the Freundlich models; Figure S2: Residuals plot for the kinetic profiles reported in Figure 6 fitted by Pseudo-first order and Double Exponential Models.

Funding: This research was financially supported by MIUR and by Progetto di ricerca e sviluppo “AGM for CuHe” (ARS01_00697) and the University of Palermo.

Conflicts of Interest: The author declares no conflict of interest.

References

1. Bhattacharya, S.; Gupta, A.; Gupta, A.; Pandey, A. Introduction to Water Remediation: Importance and Methods. In *Water Remediation*; Springer Nature: Singapore, 2018; pp. 3–8. ISBN 978-981-10-7550-6.
2. Camera-Roda, G.; Loddo, V.; Palmisano, L.; Parrino, F. Photocatalytic ozonation for a sustainable aquaculture: A long-term test in a seawater aquarium. *Appl. Catal. B Environ.* **2019**, *253*, 69–76. [[CrossRef](#)]
3. Hao, X.; Wang, X.; Liu, R.; Li, S.; van Loosdrecht, M.C.M.; Jiang, H. Environmental impacts of resource recovery from wastewater treatment plants. *Water Res.* **2019**, *160*, 268–277. [[CrossRef](#)]
4. Parrino, F.; Camera-Roda, G.; Loddo, V. Palmisano Three-Dimensional Calibration for Routine Analyses of Bromide and Nitrate Ions as Indicators of Groundwater Quality in Coastal Territories. *Int. J. Environ. Res. Public Health* **2019**, *16*, 1419. [[CrossRef](#)]
5. Toledano Garcia, D.; Ozer, L.Y.; Parrino, F.; Ahmed, M.; Brudecki, G.P.; Hasan, S.W.; Palmisano, G. Photocatalytic ozonation under visible light for the remediation of water effluents and its integration with an electro-membrane bioreactor. *Chemosphere* **2018**, *209*, 534–541. [[CrossRef](#)]
6. Calabrese, I.; Cavallaro, G.; Lazzara, G.; Merli, M.; Sciascia, L.; Turco Liveri, M.L. Preparation and characterization of bio-organoclays using nonionic surfactant. *Adsorption* **2016**, *22*, 105–116. [[CrossRef](#)]
7. Cataldo, S.; Cavallaro, G.; Gianguzza, A.; Lazzara, G.; Pettignano, A.; Piazzese, D.; Villaescusa, I. Kinetic and equilibrium study for cadmium and copper removal from aqueous solutions by sorption onto mixed alginate/pectin gel beads. *J. Environ. Chem. Eng.* **2013**, *1*, 1252–1260. [[CrossRef](#)]
8. Jaspal, D.; Malviya, A. Composites for wastewater purification: A review. *Chemosphere* **2020**, *246*, 125788. [[CrossRef](#)]

9. Sadraei, R.; Paganini, M.C.; Calza, P.; Magnacca, G. An Easy Synthesis for Preparing Bio-Based Hybrid Adsorbent Useful for Fast Adsorption of Polar Pollutants. *Nanomaterials* **2019**, *9*, 731. [[CrossRef](#)]
10. Singh, S.; Kumar, V.; Datta, S.; Dhanjal, D.S.; Sharma, K.; Samuel, J.; Singh, J. Current advancement and future prospect of biosorbents for bioremediation. *Sci. Total Environ.* **2020**, *709*, 135895. [[CrossRef](#)]
11. Wang, J.; Zhuang, S. Removal of various pollutants from water and wastewater by modified chitosan adsorbents. *Crit. Rev. Environ. Sci. Technol.* **2017**, *47*, 2331–2386. [[CrossRef](#)]
12. Wang, W.; Hu, B.; Wang, C.; Liang, Z.; Cui, F.; Zhao, Z.; Yang, C. Cr(VI) removal by micron-scale iron-carbon composite induced by ball milling: The role of activated carbon. *Chem. Eng. J.* **2020**, *389*, 122633. [[CrossRef](#)]
13. Zhao, S.; Bai, Z.; Wang, B.; Tian, T.; Hu, Z. Innovative benign-to-design functionalized adsorbents from biomass for rapid azo-dyes separation. *Sep. Purif. Technol.* **2020**, *241*, 116633. [[CrossRef](#)]
14. Cuevas, J.; Dirocie, N.; Yunta, F.; García Delgado, C.; González Santamaría, E.D.; Ruiz, I.A.; Fernández, R.; Eymar, E. Evaluation of the Sorption Potential of Mineral Materials Using Tetracycline as a Model Pollutant. *Minerals* **2019**, *9*, 453. [[CrossRef](#)]
15. Kozera-Sucharda, B.; Gworek, B.; Kondzielski, I. The Simultaneous Removal of Zinc and Cadmium from Multicomponent Aqueous Solutions by Their Sorption onto Selected Natural and Synthetic Zeolites. *Minerals* **2020**, *10*, 343. [[CrossRef](#)]
16. Mukhopadhyay, R.; Bhaduri, D.; Sarkar, B.; Rusmin, R.; Hou, D.; Khanam, R.; Sarkar, S.; Kumar Biswas, J.; Vithanage, M.; Bhatnagar, A.; et al. Clay–polymer nanocomposites: Progress and challenges for use in sustainable water treatment. *J. Hazard. Mater.* **2020**, *383*, 121125. [[CrossRef](#)]
17. Bertolino, V.; Cavallaro, G.; Lazzara, G.; Milioto, S.; Parisi, F. Biopolymer-Targeted Adsorption onto Halloysite Nanotubes in Aqueous Media. *Langmuir* **2017**, *33*, 3317–3323. [[CrossRef](#)]
18. Cataldo, S.; Lazzara, G.; Massaro, M.; Muratore, N.; Pettignano, A.; Riela, S. Functionalized halloysite nanotubes for enhanced removal of lead(II) ions from aqueous solutions. *Appl. Clay Sci.* **2018**, *156*, 87–95. [[CrossRef](#)]
19. Cavallaro, G.; Lazzara, G.; Milioto, S.; Parisi, F.; Sanzillo, V. Modified Halloysite Nanotubes: Nanoarchitectures for Enhancing the Capture of Oils from Vapor and Liquid Phases. *ACS Appl. Mater. Interfaces* **2014**, *6*, 606–612. [[CrossRef](#)]
20. Lvov, Y.; Aerov, A.; Fakhrullin, R. Clay nanotube encapsulation for functional biocomposites. *Adv. Colloid Interface Sci.* **2013**, *207*. [[CrossRef](#)]
21. Ahmad, S.Z.N.; Wan Salleh, W.N.; Ismail, A.F.; Yusof, N.; Mohd Yusop, M.Z.; Aziz, F. Adsorptive removal of heavy metal ions using graphene-based nanomaterials: Toxicity, roles of functional groups and mechanisms. *Chemosphere* **2020**, *248*, 126008. [[CrossRef](#)]
22. Jawed, A.; Saxena, V.; Pandey, L.M. Engineered nanomaterials and their surface functionalization for the removal of heavy metals: A review. *J. Water Process Eng.* **2020**, *33*, 101009. [[CrossRef](#)]
23. Louati, I.; Elloumi-Mseddi, J.; Cheikhrouhou, W.; Hadrich, B.; Nasri, M.; Aifa, S.; Woodward, S.; Mechichi, T. Simultaneous cleanup of Reactive Black 5 and cadmium by a desert soil bacterium. *Ecotoxicol. Environ. Saf.* **2020**, *190*, 110103. [[CrossRef](#)]
24. Marian, L.; Rotaru, A.; Pălărie, I.; Moanță, A.; Popescu, M.; Morîntale, E.; Bubulică, M.; Florian, G.; Harabor, A.; Rotaru, P. Tartrazine: Physical, thermal and biophysical properties of the most widely employed synthetic yellow food-colouring azo dye. *J. Therm. Anal. Calorim.* **2018**, *134*, 209–231. [[CrossRef](#)]
25. Negrea, A.; Gabor, A.; Davidescu, C.M.; Ciopec, M.; Negrea, P.; Duteanu, N.; Barbulescu, A. Rare Earth Elements Removal from Water Using Natural Polymers. *Sci. Rep.* **2018**, *8*, 316. [[CrossRef](#)]
26. Politi, D.; Sidiras, D. Wastewater Treatment for Dyes and Heavy Metals Using Modified Pine Sawdust as Adsorbent. *Procedia Eng.* **2012**, *42*, 1969–1982. [[CrossRef](#)]
27. Rotaru, A.; Moanță, A.; Constantinescu, C.-D.; Dumitru, M.; Manolea, H.; Andreea Carmen, A.; Dinescu, M. Thermokinetic study of CODA azoic liquid crystal and thin films deposition by matrix-assisted pulsed laser evaporation. *J. Therm. Anal. Calorim.* **2017**, *128*, 89–105. [[CrossRef](#)]
28. Rotaru, A.; Brătulescu, G.; Rotaru, P. Thermal analysis of azoic dyes: Part I. Non-isothermal decomposition kinetics of [4-(4-chlorobenzoyloxy)-3-methylphenyl](p-tolyl)diazene in dynamic air atmosphere. *Thermochim. Acta* **2009**, *489*, 63–69. [[CrossRef](#)]
29. Rotaru, A.; Moanță, A.; Rotaru, P.; Segal, E. Thermal decomposition kinetics of some aromatic azomonoethers: Part III. Non-isothermal study of 4-[(4-chlorobenzyl)oxy]-4'-chloroazobenzene in dynamic air atmosphere. *J. Therm. Anal. Calorim.* **2009**, *95*, 161–166. [[CrossRef](#)]

30. Rotaru, A.; Constantinescu, C.-D.; Rotaru, P.; Moanță, A.; Dumitru, M.; Socaciu, M.; Maria, D.; Segal, E. Thermal analysis and thin films deposition by matrix assisted pulsed laser evaporation of a 4CN type azomonoether. *J. Therm. Anal. Calorim.* **2008**, *92*, 279–284. [[CrossRef](#)]
31. Rotaru, A.; Dumitru, M. Thermal behaviour of CODA azoic dye liquid crystal and nanostructuring by drop cast and spin coating techniques. *J. Therm. Anal. Calorim.* **2017**, *127*, 21–32. [[CrossRef](#)]
32. Varrica, D.; Tamburo, E.; Milia, N.; Vallascas, E.; Cortimiglia, V.; De Giudici, G.; Dongarrà, G.; Sanna, E.; Monna, F.; Losno, R. Metals and metalloids in hair samples of children living near the abandoned mine sites of Sulcis-Inglesiente (Sardinia, Italy). *Environ. Res.* **2014**, *134*, 366–374. [[CrossRef](#)]
33. Visa, M.; Bogatu, C.; Duta, A. Simultaneous adsorption of dyes and heavy metals from multicomponent solutions using fly ash. *Appl. Surf. Sci.* **2010**, *256*, 5486–5491. [[CrossRef](#)]
34. Sarma, G.K.; SenGupta, S.; Bhattacharyya, K.G. Adsorption of Monoazo Dyes (Crocein Orange G and Procion Red MX5B) from Water Using Raw and Acid-Treated Montmorillonite K10: Insight into Kinetics, Isotherm, and Thermodynamic Parameters. *Water. Air. Soil Pollut.* **2018**, *229*, 312. [[CrossRef](#)]
35. Sciascia, L.; Casella, S.; Cavallaro, G.; Lazzara, G.; Milioto, S.; Princivalle, F.; Parisi, F. Olive mill wastewaters decontamination based on organo-nano-clay composites. *Thermophys. Asp. Funct. Ceram. Surf.* **2019**, *45*, 2751–2759. [[CrossRef](#)]
36. Sharma, P.; Borah, D.J.; Das, P.; Das, M.R. Cationic and anionic dye removal from aqueous solution using montmorillonite clay: Evaluation of adsorption parameters and mechanism. *Desalin. Water Treat.* **2016**, *57*, 8372–8388. [[CrossRef](#)]
37. Zhang, Q.; Jing, R.; Zhao, S.; Wu, M.; Liu, X.; Shao, Y.; Lv, F.; Liu, A.; Meng, Z. Adsorption of cationic and anionic dyes on montmorillonite in single and mixed wastewater. *J. Porous Mater.* **2019**, *26*, 1861–1867. [[CrossRef](#)]
38. Liu, X.; Zhou, F.; Chi, R.; Feng, J.; Ding, Y.; Liu, Q. Preparation of Modified Montmorillonite and Its Application to Rare Earth Adsorption. *Minerals* **2019**, *9*, 747. [[CrossRef](#)]
39. Parisi, F.; Lazzara, G.; Merli, M.; Milioto, S.; Princivalle, F.; Sciascia, L. Simultaneous Removal and Recovery of Metal Ions and Dyes from Wastewater through Montmorillonite Clay Mineral. *Nanomaterials* **2019**, *9*, 1699. [[CrossRef](#)]
40. Rojas, J.; Suarez, D.; Moreno, A.; Silva-Agredo, J.; Torres-Palma, R. Kinetics, Isotherms and Thermodynamic Modeling of Liquid Phase Adsorption of Crystal Violet Dye onto Shrimp-Waste in Its Raw, Pyrolyzed Material and Activated Charcoals. *Appl. Sci.* **2019**, *9*, 5337. [[CrossRef](#)]
41. Varshini, J.S.; Das, D.; Das, N. Packed bed column studies on recovery of cerium(III) from electronic wastewater using biosorbents of animal and plant origin. *Indian J. Chem. Technol.* **2017**, *24*, 294–303.
42. Dubey, S.S.; Rao, B.S. Removal of cerium ions from aqueous solution by hydrous ferric oxide – A radiotracer study. *J. Hazard. Mater.* **2011**, *186*, 1028–1032. [[CrossRef](#)] [[PubMed](#)]
43. Duraipandian, J.; Rengasamy, T.; Vadivelu, S. Experimental and Modeling Studies for the Removal of Crystal Violet Dye from Aqueous Solutions using Eco-friendly Gracilaria corticata Seaweed Activated Carbon/Zn/Alginate Polymeric Composite Beads. *J. Polym. Environ.* **2017**, *25*, 1062–1071. [[CrossRef](#)]
44. Hayati, B.; Maleki, A.; Najafi, F.; Daraei, H.; Gharibi, F.; McKay, G. Super high removal capacities of heavy metals (Pb²⁺ and Cu²⁺) using CNT dendrimer. *J. Hazard. Mater.* **2017**, *336*, 146–157. [[CrossRef](#)] [[PubMed](#)]
45. He, H.; Yang, S.; Yu, K.; Ju, Y.; Sun, C.; Wang, L. Microwave induced catalytic degradation of crystal violet in nano-nickel dioxide suspensions. *J. Hazard. Mater.* **2010**, *173*, 393–400. [[CrossRef](#)] [[PubMed](#)]
46. Karimi, H. Effect of pH and Initial pb(II) Concentration on The Lead Removal Efficiency from Industrial Wastewater Using Ca(OH)₂. *Int. J. Water Wastewater Treat.* **2017**, *3*. [[CrossRef](#)]
47. Varrica, D.; Dongarrà, G.; Alaimo, M.G.; Monna, F.; Losno, R.; Sanna, E.; De Giudici, G.; Tamburo, E. Lead isotopic fingerprint in human scalp hair: The case study of Iglesias mining district (Sardinia, Italy). *Sci. Total Environ.* **2018**, *613–614*, 456–461. [[CrossRef](#)]
48. Ain, Q.U.; Zhang, H.; Yaseen, M.; Rasheed, U.; Liu, K.; Subhan, S.; Tong, Z. Facile fabrication of hydroxyapatite-magnetite-bentonite composite for efficient adsorption of Pb(II), Cd(II), and crystal violet from aqueous solution. *J. Clean. Prod.* **2020**, *247*, 119088. [[CrossRef](#)]
49. Deng, J.; Liu, Y.; Liu, S.; Zeng, G.; Tan, X.; Huang, B.; Tang, X.; Wang, S.; Hua, Q.; Yan, Z. Competitive adsorption of Pb(II), Cd(II) and Cu(II) onto chitosan-pyromellitic dianhydride modified biochar. *J. Colloid Interface Sci.* **2017**, *506*, 355–364. [[CrossRef](#)]

50. Filipi, R.; Nesmerak, K.; Rucki, M.; Roth, Z.; Hanzlikova, I.; Tichý, M. Acute toxicity of rare earth elements and their compounds. *Chem. Listy* **2007**, *101*, 793–798.
51. Masoumi, A.; Hemmati, K.; Ghaemy, M. Low-cost nanoparticles sorbent from modified rice husk and a copolymer for efficient removal of Pb(II) and crystal violet from water. *Chemosphere* **2016**, *146*, 253–262. [[CrossRef](#)]
52. Zeng, Q.; Huang, Y.; Huang, L.; Li, S.; Hu, L.; Xiong, D.; Zhong, H.; He, Z. A novel composite of SiO₂ decorated with nano ferrous oxalate (SDNF) for efficient and highly selective removal of Pb²⁺ from aqueous solutions. *J. Hazard. Mater.* **2020**, *391*, 122193. [[CrossRef](#)]
53. Moja, T.N.; Bunekar, N.; Mishra, S.B.; Tsai, T.-Y.; Hwang, S.S.; Mishra, A.K. Melt processing of polypropylene-grafted-maleic anhydride/Chitosan polymer blend functionalized with montmorillonite for the removal of lead ions from aqueous solutions. *Sci. Rep.* **2020**, *10*. [[CrossRef](#)] [[PubMed](#)]
54. Gupt, C.B.; Bordoloi, S.; Sekharan, S.; Sarmah, A.K. Adsorption characteristics of Barmer bentonite for hazardous waste containment application. *J. Hazard. Mater.* **2020**, *396*, 122594. [[CrossRef](#)] [[PubMed](#)]
55. Doi, A.; Khosravi, M.; Ejtemaei, M.; Nguyen, T.A.H.; Nguyen, A.V. Specificity and affinity of multivalent ions adsorption to kaolinite surface. *Appl. Clay Sci.* **2020**, *190*, 105557. [[CrossRef](#)]
56. Imam, D.M.; Rizk, S.E.; Attallah, M.F. Adsorption studies of Ce(III) and Zr(IV) from aqueous solution using clay and humic acid—Clay materials. *Part. Sci. Technol.* **2019**. [[CrossRef](#)]
57. Chenab, K.K.; Sohrabi, B.; Jafari, A.; Ramakrishna, S. Water treatment: Functional nanomaterials and applications from adsorption to photodegradation. *Mater. Today Chem.* **2020**, *16*, 100262. [[CrossRef](#)]
58. Puri, C.; Sumana, G. Highly effective adsorption of crystal violet dye from contaminated water using graphene oxide intercalated montmorillonite nanocomposite. *Appl. Clay Sci.* **2018**, *166*, 102–112. [[CrossRef](#)]
59. Claver, C.; Fernández, E.; Margalef-Català, R.; Medina, F.; Salagre, P.; Sueiras, J.E. Studies on the Characterization of Several Iridium- and Rhodium-clay Catalysts and Their Activity in Imine Hydrogenation. *J. Catal.* **2001**, *201*, 70–79. [[CrossRef](#)]
60. Dawodu, F.; Akpomie, K.; Abuh, M. Equilibrium Isotherm Studies on the Batch Sorption of Copper (II) ions from Aqueous Solution unto Nsu Clay. *Int. J. Sci. Eng. Res.* **2012**, *3*, 1–7.
61. Brigatti, M.F.; Corradini, F.; Franchini, G.C.; Mazzoni, S.; Medici, L.; Poppi, L. Interaction between montmorillonite and pollutants from industrial waste-waters: Exchange of Zn²⁺ and Pb²⁺ from aqueous solutions. *Appl. Clay Sci.* **1995**, *9*, 383–395. [[CrossRef](#)]
62. Oueslati, W.; Mefath, M.; ben rhaïem, H.; Ben Haj Amara, A. Cation Exchange Selectivity versus concentration of competing heavy metal cations (Pb²⁺, Zn²⁺): Case of Na-montmorillonite. *Phys. Procedia* **2009**, *2*, 1059–1063. [[CrossRef](#)]
63. Marsh, A.; Heath, A.; Patureau, P.; Evernden, M.; Walker, P. Alkali activation behaviour of un-calcined montmorillonite and illite clay minerals. *Appl. Clay Sci.* **2018**, *166*, 250–261. [[CrossRef](#)]
64. Harun, F.; Almadani, E.; Radzi, S. Metal cation exchanged montmorillonite K10 (MMT K10): Surface properties and catalytic activity. *J. Sci. Res. Dev.* **2016**, *3*, 90–96.
65. Zhang, S.Q.; Hou, W.G. Adsorption behavior of Pb(II) on montmorillonite. *Colloids Surf. Physicochem. Eng. Asp.* **2008**, *320*, 92–97. [[CrossRef](#)]
66. Fang, Z.; Liu, B.; Luo, J.; Ren, Y.; Zhang, Z. Efficient conversion of carbohydrates into 5-hydroxymethylfurfural catalyzed by the chromium-exchanged montmorillonite K-10 clay. *Biomass Bioenergy* **2014**, *60*, 171–177. [[CrossRef](#)]
67. Gupta, S.; Bhattacharyya, K. Adsorption of heavy metals on kaolinite and montmorillonite: A review. *Phys. Chem. Chem. Phys.* **2012**, *14*, 6698–6723. [[CrossRef](#)]

